

Systematic Review of Pituitary Gland and Pituitary Adenoma Automatic Segmentation Techniques in Magnetic Resonance Imaging

Mubaraq Yakubu^{1, 2, 3*}, Navodini Wijithilake⁴,
Jonathan Shapey⁴, Andrew King⁴, Alexander Hammers^{1, 5, 6}

¹*King's College London & Guy's and St Thomas' PET Centre, King's College London, Westminster Bridge Rd, London, SE1 7EH, Greater London, United Kingdom.

²Radiology Department, Aminu Kano Teaching Hospital, Zaria Rd, Kano, 700233, Kano, Nigeria.

³Medical Artificial Intelligence (MAI) Lab, Crestview Radiology-NOHIL CT and MRI Centre, Igbobi, Ikeja-Main Land, 100252, Lagos, Nigeria.

⁴Biomedical Engineering and Imaging Science, King's College London, Lambeth Palace Rd, London, SE1 7EU, Greater London, United Kingdom.

⁵Research Department of Biomedical Computing, School of Biomedical Engineering and Imaging Sciences, King's College London, Westminster Bridge Rd, London, SE1 7EH, Greater London, UK.

⁶Research Department of Early Life Imaging, School of Biomedical Engineering and Imaging Sciences, King's College London, Westminster Bridge Rd, London, SE1 7EH, Greater London, UK.

*Corresponding author(s). E-mail(s): mubaraq.yakubu@kcl.ac.uk;
Contributing authors: navodini.wijethilake@kcl.ac.uk;
Jonathan.Shapey@kcl.ac.uk; andrew.king@kcl.ac.uk;
alexander.hammers@kcl.ac.uk;

Abstract

Purpose: Accurate segmentation of both the pituitary gland and adenomas from magnetic resonance imaging (MRI) is essential for diagnosis and treatment of pituitary adenomas. This systematic review evaluates automatic segmentation

methods for improving the accuracy and efficiency of MRI-based segmentation of pituitary adenomas and the gland itself. **Methods:** We reviewed 34 studies that employed automatic and semi-automatic segmentation methods. We extracted and synthesized data on segmentation techniques and performance metrics (such as Dice overlap scores). **Results:** The majority of reviewed studies utilized deep learning approaches, with U-Net-based models being the most prevalent. Automatic methods yielded Dice scores of 0.19–89.00% for pituitary gland and 4.60–96.41% for adenoma segmentation. Semi-automatic methods reported 80.00–92.10% for pituitary gland and 75.90–88.36% for adenoma segmentation. **Conclusion:** Most studies did not report important metrics such as MR field strength, age and adenoma size. Automated segmentation techniques such as U-Net-based models show promise, especially for adenoma segmentation, but further improvements are needed to achieve consistently good performance in small structures like the normal pituitary gland. Continued innovation and larger, diverse datasets are likely critical to enhancing clinical applicability.

Keywords: Pituitary Adenoma, Pituitary Gland, Magnetic Resonance Imaging (MRI), Automatic Segmentation, Deep Learning, UNet, Semi-Automatic Segmentation

1 Introduction

Pituitary adenomas (PAs), also known as pituitary neuroendocrine tumours [1], are heterogeneous slow-growing brain tumours caused by abnormal growth of the pituitary gland (PG). PAs are common (14% in autopsy studies) [2], but almost all are benign [3]. Functional PAs, often microadenomas (<1 cm), may cause debilitating hormonal disorders such as Cushing's disease [4], while larger, non-functional macroadenomas (>1 cm) and giant PAs (>4 cm) can exert mass effects, leading to headaches and visual disturbances by compressing structures like the optic chiasm and cavernous sinus [5–8].

Clinical investigation of PAs involves the use of magnetic resonance imaging (MRI) of the pituitary region [9]. Common MRI sequences for imaging PAs include T1-weighted, T2-weighted, and Fluid Attenuated Inverted Recovery (FLAIR) [10]. Contrast medium, such as gadolinium-DTPA, is often used, with a standard dose of 0.1 mmol/kg, to improve delineation of PAs and surrounding structures, particularly in small functional PAs [11, 12]. T1-weighted (with and without contrast) and T2-weighted MRI sequences provide satisfactory visualization of pituitary adenomas in most cases [13]. There have been reported differences in the MRI appearance of different types and stages of PAs in MRI images acquired by different sequences and pre/post contrast [14]. However, unlike other brain conditions, PA suffers from a lack of publicly accessible data to support research and model development. A notable exception is the Cheng 2015 dataset [15], also referred to as the Figshare dataset [16]. Several techniques have been employed to segment anatomical structures. Traditional methods such as thresholding, region growing, region merging and splitting, clustering, edge detection, atlasing and model-based approaches have laid the foundation for

automated or semi-automated image segmentation [17]. The rise of deep learning techniques has revolutionized the automatic segmentation of medical images, especially for brain tumors like PAs [18]. A recent review highlighted the prominence of U-Net [19], a deep learning-based fully convolutional network, and its variants demonstrating superior performance in brain tumor segmentation tasks [20]. This shift towards deep learning-based techniques is driven by the need for more accurate, precise and efficient approaches to the diagnosis and treatment planning of PAs [21].

We found significant variation in the methodological approaches, model types, and reporting of findings across studies related to the automatic segmentation of normal PG and PA in MRI. This review explores and systematically integrates these varied perspectives comprehensively, providing a broader understanding of the current state of the field and explored how accurate automated segmentation algorithms for PG and PA are. The main aim of this work is to systematically review the available literature on automatic segmentation of PG and PA that used magnetic resonance images.

2 Methods

The systematic review was conducted in accordance with PRISMA guidelines [22].

2.1 Eligibility Criteria

Articles that focus on improved PG or PA segmentation using MRI to enable accurate diagnosis are the main focus of this systematic review. All articles that met the following inclusion criteria were reviewed:

1. Full length peer-reviewed articles on pituitary imaging segmentation.
2. Description of an automated machine learning or deep learning algorithm for the segmentation of MRI images specifically targeting the pituitary or sellar region.

We excluded case reports, literature reviews, conference abstracts, book chapters, meta-analyses, and editorials as well as articles that did not mention the use of manual and automatic segmentation or MR acquisition protocol in patients with PA or PG imaging. The information sources including search strategy and other data collection processes are available in the supplementary material.

3 Results

3.1 Study Selection

3.1.1 Search and Selection Process

The detailed processes are summarized in Figures 1 and 2.

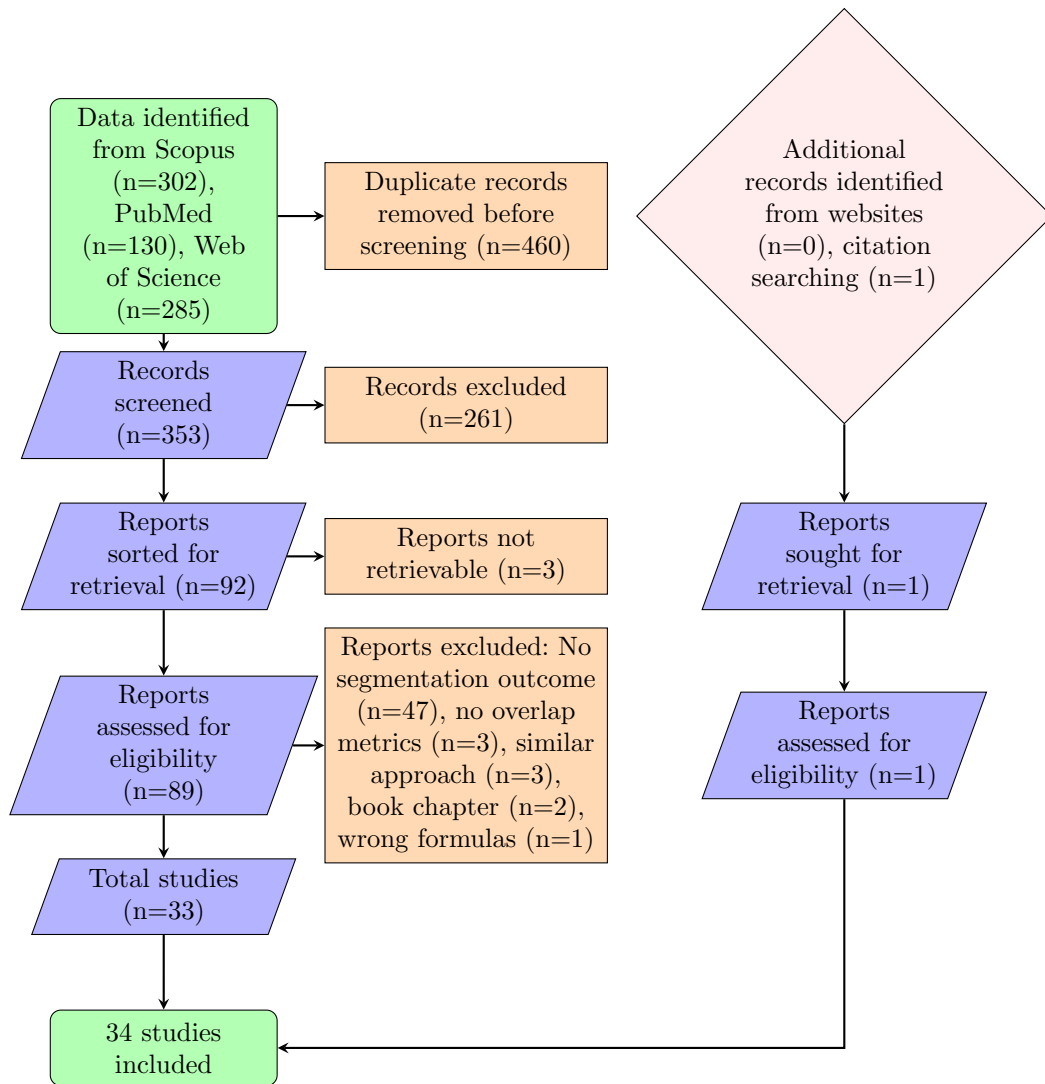


Fig. 1: Flowchart of the search and selection process for study inclusion

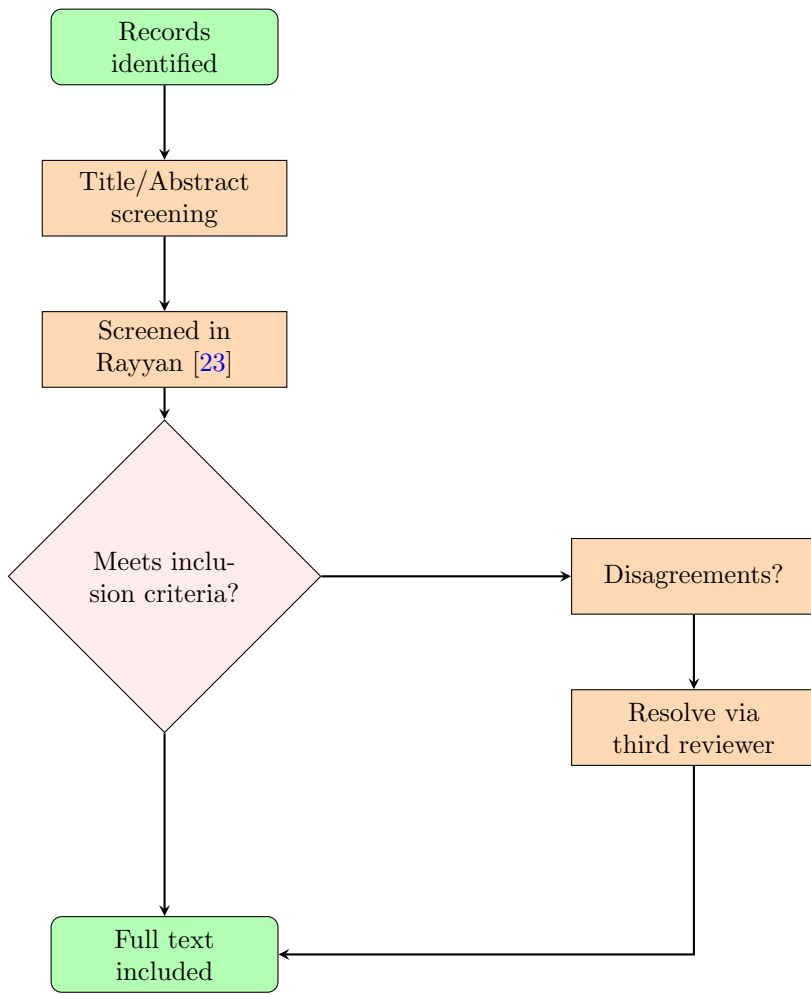


Fig. 2: Selection process for inclusion of studies

3.1.2 Segmentation Approaches for Pituitary Gland MRI Studies

To categorize the segmentation techniques used in the selected studies, we classified them based on the level of automation and the methods employed. The segmentation strategies are shown in Figure 3.

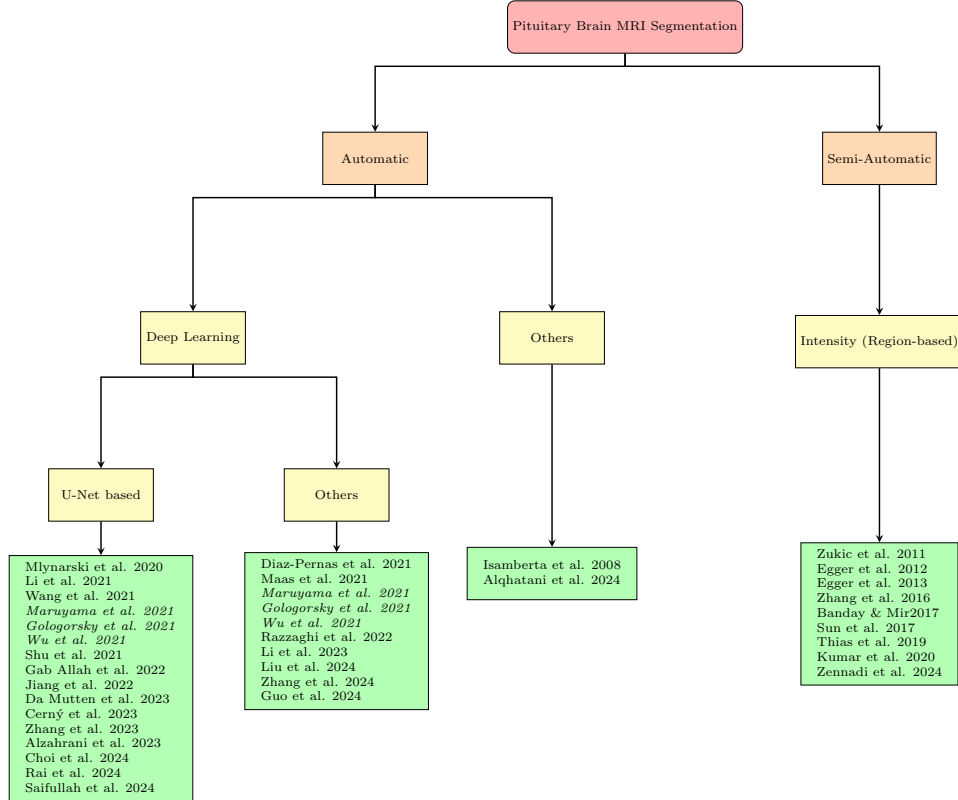


Fig. 3: Segmentation approaches for pituitary MRI Studies. Studies in *italics* utilized both U-Net and other Deep Learning methods, i.e. are listed twice

3.2 Study Characteristics

A total of 34 studies were included in this review, each focusing on different segmentation approaches and MRI modalities, characterized as follows:

Segmentation Approaches: 13 studies employed purely **UNet-based models** for segmentation, three used a combination of **UNet-based** and other deep learning models, eight explored **other deep learning models**, two applied an automatic segmentation approach without **deep learning**, and eight utilized **semi-automatic approaches**.

MRI Field Strength: six studies used 1.5T MRI scans, two studies used 3T MRI scans, five studies used both 1.5T and 3T scans, one study used 1T, 1.5T and 3T, and the remaining 20 studies did not specify the MRI field strength, including nine of the reviewed studies that utilized the *Cheng 2015 dataset* [15].

3.2.1 Cheng Dataset Description

The *Cheng 2015 dataset* [15] provides T1-weighted contrast-enhanced MRI scans of the pituitary region. The full dataset consists of 3064 slices from 233 patients and includes three types of brain tumors: 930 PA, 708 meningioma, and 1426 glioma slices. The images were acquired between September 2005 and October 2010 at Nanfang Hospital (Guangzhou, China) and the General Hospital of Tianjin Medical University (Tianjin, China). Each scan has an in-plane resolution of 512×512 pixels, with a pixel spacing of $0.49 \times 0.49 \text{ mm}^2$, a slice thickness of 6 mm, and an inter-slice gap of 1 mm. A gadolinium-based contrast agent (Gd-DTPA) was administered at a standard dose of 0.1 mmol/kg at an injection rate of 2 ml/s.

3.3 Results of Individual Studies

The results are categorized based on the type of segmentation models used and further subdivided based on their application to PG and PA. Performance metrics, such as Dice Similarity Coefficient and other relevant findings, are summarized in Tables 1, 2, 3, and 4. Studies included by inclusion criteria but which were later excluded can be found in Appendix A.

Table 1: Outcome of Automatic PG Segmentation Studies

Study	Dataset Used	MRI Strength (Tesla)	MS Soft	Ground Truth (Images)	Models Used	Model Number	Model Description	2D vs. 3D	Dice
[24]	Local	1.5	N/A	11	1	1	ABAS	2D	30.00
[25]	Local	N/A	N/A	29	1	1	Modified 2D U-Net (OVMA)	2D	79.70
[26]	Local	3.0	ITK-Snap	213	1	1	Gated-shaped U-Net	2D	60.00
[27]	ADNI	1.5 & 3.0	MATLAB Image Labeler	450	6	1	AlexNet	2D	46.86
∞	[28]	ABIDE	N/A	3D Slicer	333	7	UNET3D VNET CONDSEG OBELISK 96 OBELISK 144 UNETR Ensemble	2D	79.10 77.10 79.30 75.20 74.50 72.00 79.60
[29]	Local	1.5 & 3.0	ITK-snap software	521	1	1	U-Net	3D	61.10
[30]	Local	N/A	N/A	32	3	1	U-Net-MRIu U-Net-MRIeCT U-Net-MRIeMRI	3D	35.00 32.00 67.00
[31]	Local	3.0	ITK-Snap	153	1	1	3D U-Net	3D	89.00
[32]	Local	3.0 & 1.5	N/A	195	1	1	CAiLN	2D	84.02
[33]	Local	3.0 & 1.5	ITK-Snap	2586	1	1	Mask R-CNN	2D	47.77

2D: Two-Dimensional, 3D: Three-Dimensional, ABAS: Atlas-based automatic segmentation software, ABIDE: Autism Brain Imaging Data Exchange, ADNI: Alzheimer's Disease Neuroimaging Initiative, CAiLN: Channel Attention (Long-Short-Term-Memory) Network, CONDSEG: Conditional Segmentation, MS Soft: Manual Segmentation Software, MRI: Magnetic Resonance Imaging, MSR-Net: Multi-Scale Residual Network, N/A: Not available, OBELISK: Object Boundary Extraction using Learned Image Structures, OVMA: One Voxel Mismatch Allowed, PG: Pituitary Gland, UNET3D: 3D version of U-Net, UNETR: U-Net Transformer, VNET: V-Net

Table 2: Outcome of Automatic PA Segmentation Studies

Study	Dataset Used	Adenoma Size	MRI Strength (Tesla)	MS Soft	Ground Truth Used (Images)	Model Number	Model Description	2D vs. 3D	Dice
[34]	Cheng 2015	N/A	N/A	N/A	930	1	1	Multiscale CNN	81.30
[35]	Cheng 2015	N/A	N/A	N/A	930	1	1	Modified QuickNAT	81.20
[36]	Local	Micro-PA & Macro-PA	1.5 & 3.0	MITK	185	1	1	Res U-Net	80.93
[26]	Local	N/A	3.0	ITK-Snap	213	1	1	Gated-shaped U-Net	89.80
[37]	NTUH	N/A	N/A	N/A	155	5	1	V-Net_dropout Deconvnet	2D
							2	U-Net	38.00
							3	PSPNet4	7.00
							4	DeepMedic	24.00
							5		29.00
[38]	Local	Micro, Macro & Giant PA	1.5	ITK-Snap	243	2	1	U-Net-All type PA	80.30
							2	U-Net-Primary NFPA	85.30
[39]	Cheng 2015	N/A	N/A	N/A	930	1	1	Edge U-Net	2D
[40]	Local	N/A	N/A	LabelMe	500	1	1	Modified U-Net	2D
[41]	Cheng 2015	NA	N/A	N/A	930	1	1	Multimodal CNN	91.08
[42]	Local	Micro, Macro & Giant PA	N/A	ITK-Snap	155	1	1	cfVB-Net	3D
[43]	Local	Micro, Macro & Giant PA	1, 1.5 & 3.0	N/A	213	2	1	U-Net-Preoperative	2D
							2	U-Net-Postoperative	4.60

Table 2: Outcome of Automatic PA Segmentation Studies (continued)

[29]	Local	N/A	1.5 & 3.0	ITK-Snap	521	1	1	U-Net	3D
[44]	Local	N/A	N/A	LabelMe	2000	1	1	PDC U-Net	2D
[45]	Cheng 2015	N/A	N/A	N/A	930	1	1	EfficientNet	2D
[46]	Cheng 2015	N/A	N/A	N/A	930	1	1	FCM	2D
[47]	Local	N/A	N/A	LabelMe	2105	1	1	MSR-Net	2D
[48]	Cheng 2015	N/A	N/A	N/A	930	1	1	Modified CNN-U-Net framework	2D
[33]	Local	N/A	3.0 and 1.5	ITK-Snap	1617	1	1	Mask R-CNN	2D

2D: Two-Dimensional, 3D: Three-Dimensional, cfVB-Net: coarse-to-fine VB-Net, CNN: Convolutional Neural Network, FCM: Fuzzy C-Means Giant PA: Giant Adenoma, Macro-PA: Macroadenoma, Micro-PA: Microadenoma, MRI: Magnetic Resonance Imaging, MS Soft: Manual Segmentation Software, MSR-Net: Multi-Scale Residual Network, N/A: Not available, NFP: Non-Functioning Pituitary Adenoma, NTUH: National Taiwan University Hospital, PA: Pituitary Adenoma, PDC U-Net: parallel dilated convolutional network, PSPNet4: Pyramid Scene Parsing Network version 4, Res U-Net: Residual U-Net

Table 3: Outcome of Semi-Automatic PG Segmentation Studies

Study	Dataset Used	MRI Strength (Tesla)	MS Soft	Ground Truth (Images)	Models Used	Model Number	Model Description	2D vs. 3D	Dice
[49]	Local	N/A	N/A	10	1	1	MB	2D	87.00
[50]	Local	1.5	N/A	10	1	1	MB	2D	92.10
[51]	Local	1.5	SPM	100	1	1	MPA	3D	80.00

2D: Two-Dimensional, 3D: Three-Dimensional, MB: Morphological Based, MPA: Maximum Probability Atlas, MRI: Magnetic Resonance Imaging, MS Soft: Manual Segmentation Software, N/A: Not available, PG: Pituitary Gland, SPM: Statistical Parametric Mapping

Table 4: Outcome of Semi-Automatic PA Segmentation Studies

Study	Dataset Used	Adenoma Size	MRI Strength (Tesla)	MS Soft	Ground Truth (Images)	Models Used	Model Number	Model Description	2D vs. 3D	Dice
[52]	Local	N/A	N/A	N/A	10	1	1	Balloon inflation-based	2D	75.92
[53]	Local	N/A	1.5	MeVisLab	10	1	1	Grow-Cut In Slicer	2D & 3D	81.97
[54]	Local	N/A	1.5	N/A	10	2	1	Graph-based Balloon inflation-based	2D	77.50 75.90
[55]	N/A	N/A	N/A	ITK-Snap	23	1	1	Random Walk & Graph-Cut-Based Active Contour	2D	88.36
[56]	Cheng 2015	N/A	N/A	N/A	915	3	1	SAC	2D	83.76
[57]	Cheng 2015	N/A	N/A	N/A	930	1	1	MACWE MGAC		83.76 84.39
								Edge based contouring	2D	83.95

2D: Two-Dimensional, 3D: Three-Dimensional, MACWE: Morphological Active Contour Without Edge, MGAC: Morphological Geodesic Active Contour, MRI: Magnetic Resonance Imaging, MS Soft: Manual Segmentation Software, PA: Pituitary Adenoma, SAC: Snake Active Contour

3.4 Results of Synthesis

3.4.1 Summary of Study Characteristics

The distribution of the number and type of included segmentation studies per year is shown in Figure 4. The most commonly used approach was deep learning-based automatic segmentation, particularly U-Net models.

Figure 5 presents a box plot summarizing the distribution of Dice scores across four segmentation categories: automatic PG, automatic PA, semi-automatic PG, and semi-automatic PA. Automatic PG segmentation methods reported the widest performance range, from 0.19% to 89.00%, while one automatic PA segmentation method showed the highest overall score, reaching 96.41%. Semi-automatic methods exhibited tighter performance distributions, with PG segmentation performance ranging from 80.00% to 92.10% and PA segmentation from 75.90% to 88.36%.

Figure 6 presents a comparison of Dice scores achieved by U-Net-based and non-U-Net-based models for both pituitary gland (PG) and pituitary adenoma (PA) segmentation. These comparisons are based on the highest Dice score reported by each study for the respective model category.

Models trained on 3D data showed a wider range of Dice scores, with the highest reported value at 89.0%. In contrast, those trained on 2D data displayed a narrower spread, with scores ranging from 47.8% to 84.0%. This comparison highlights the performance variability associated with the dimensionality of the input imaging data used during model training as seen in Figure 7.

Cheng-based studies reported Dice scores within a narrower and higher range, while studies using other datasets exhibited a wider spread of Dice scores, including both lower and higher values as seen in Figure 8.

Within studies that used the *Cheng 2015 dataset* for PA segmentation, automatic methods reported Dice scores ranging from 81.20% to 96.41%, while semi-automatic methods achieved scores between 83.95% and 84.39%, Figure 9.

Statistical comparisons were conducted using the highest Dice score reported per study. Significant differences were observed in PG segmentation between automatic and semi-automatic methods, Table 5. Other comparisons, including PA segmentation methods, 2D vs. 3D input types, and dataset origin (Cheng vs. others), did not show statistically significant differences. Comparisons on field strength, age, gender, menstrual status, and pituitary or adenoma size were not possible due to insufficient reporting in the original studies.

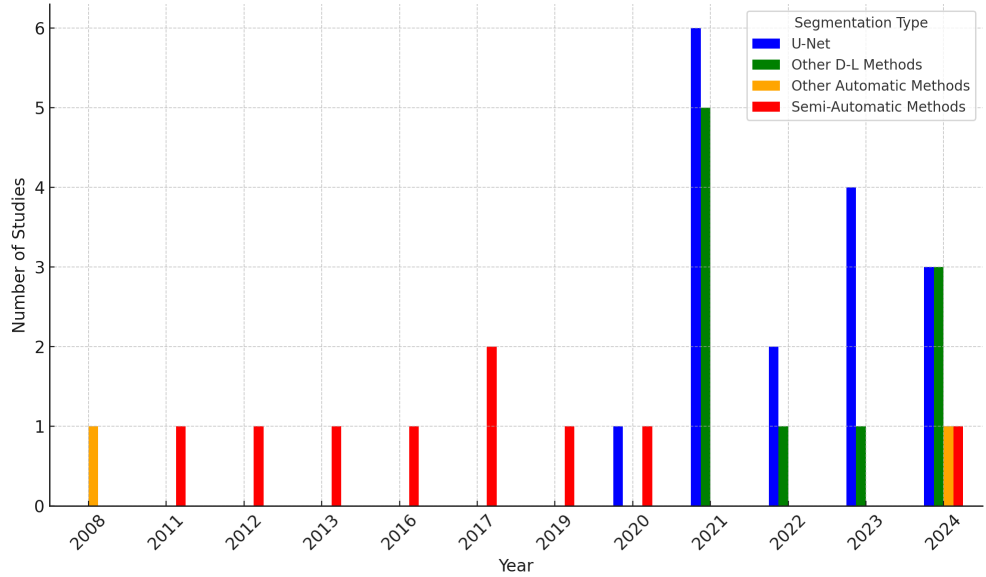


Fig. 4: Number of segmentation studies per year

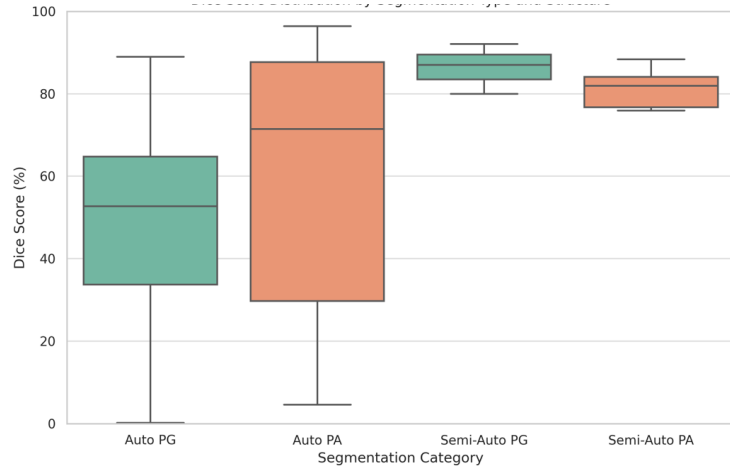


Fig. 5: Dice score distributions for automated and semi-automated segmentation methods across pituitary gland (PG) and pituitary adenoma (PA) structures. Box plot horizontal lines represent the median (center), first and third quartiles (box edges), and the minimum and maximum values within $1.5 \times$ interquartile range (whiskers). No outliers were detected in this comparison.

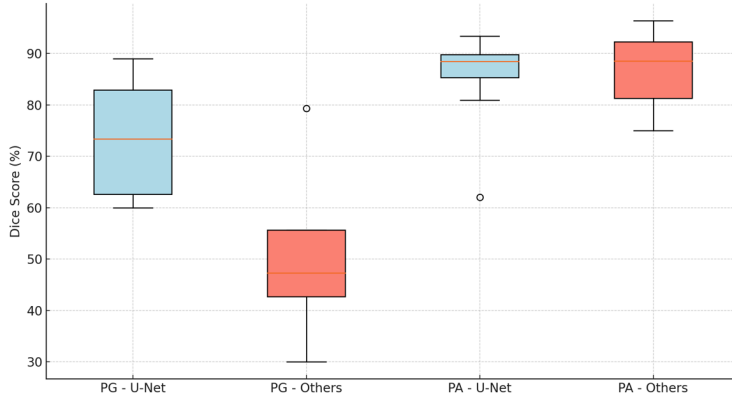


Fig. 6: Box plot comparing Dice scores for U-Net-based and non-U-Net-based models across pituitary gland (PG) and pituitary adenoma (PA) segmentation. Elements are the same as Figure 5 (dots outside the whiskers [PG-Others and PA-U-Net] represent outliers). For each study, only the highest reported Dice score was used in this comparison.

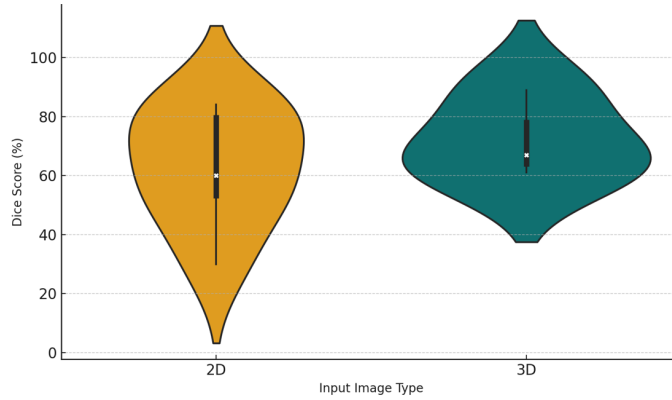


Fig. 7: Violin plots of Dice score distribution for PG automatic segmentation comparing 2D and 3D input image types. The width of each violin indicates the density of data points at different Dice score values. The central white dot represents the median, the thick black bar is the interquartile range, and the thin black line shows the range within $1.5 \times$ the interquartile range. Wider sections indicate more frequent Dice scores in that range.

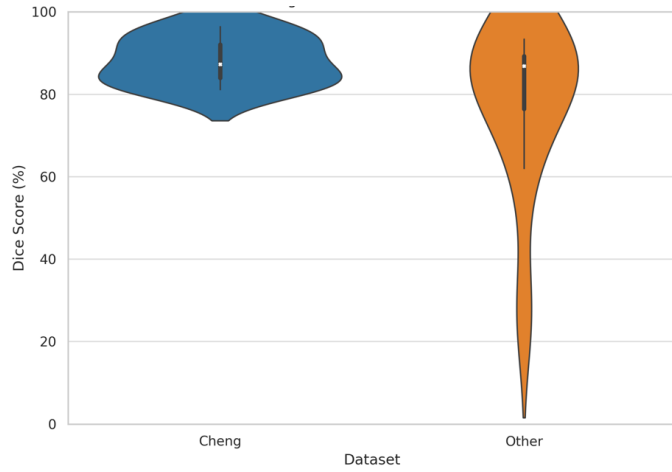


Fig. 8: Violin plots of Dice score distribution for PA automatic segmentation: Cheng 2015 dataset vs other datasets. Elements are the same as Figure 7.

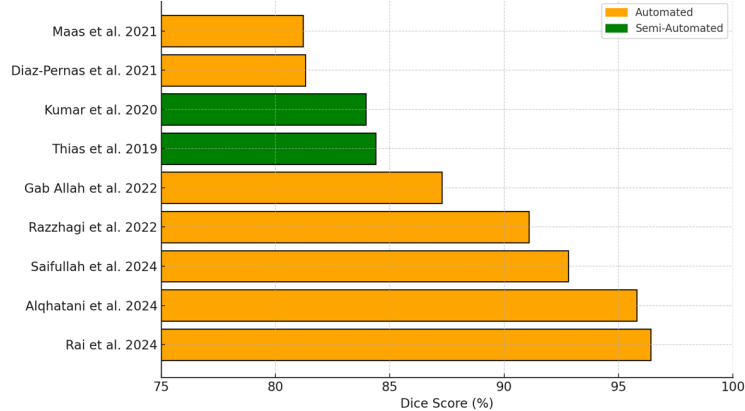


Fig. 9: Dice scores of studies that utilized the Cheng 2015 dataset for pituitary adenoma segmentation, grouped by segmentation method. Automated models demonstrated a wider and generally higher performance range compared to semi-automated methods.

3.4.2 Possible Causes of Heterogeneity Among Results

The segmentation techniques used in the included studies varied, ranging from deep learning-based models such as U-Net to region-based and active contour methods. Additionally, there were notable differences in imaging modalities, with studies using

Table 5: Statistical comparison of Dice scores across segmentation method groupings using the Mann–Whitney U (MW) and Kolmogorov–Smirnov (K–S) tests. First comparator is better.

Comparison	MW	MW p-value	K–S Statistic	K–S p-value
PG Auto vs Semi-Auto	3.0	0.049*	0.800	0.070
PA Auto vs Semi-Auto	87.0	0.158	0.524	0.085
U-Net vs Others (PG Auto)	21.0	0.329	0.600	0.238
U-Net vs Others (PA Auto)	41.0	1.000	0.222	0.989
Cheng vs Other (PA Auto)	55.0	0.151	0.481	0.208
2D vs 3D (PG Auto)	6.0	0.383	0.571	0.400
Auto vs Semi-Auto (Cheng)	10.0	0.500	0.714	0.333

* Statistically significant ($p < 0.05$)

1.5T, 3T, a combination of both, and one study employing 1T, 1.5T, and 3T MRI field strengths. However, many studies did not specify the field strength used.

3.4.3 Sensitivity Analyses Conducted

Given the heterogeneity in segmentation techniques and the lack of relevant data reported (see supplementary material), a sensitivity analysis was not feasible or relevant.

4 Discussion

4.1 Overview of Segmentation Techniques

Our review identified a variety of studies focusing on the segmentation of PA and PG using MRI. These studies can be categorized into two primary segmentation approaches: automatic and semi-automatic. Within these categories, the techniques utilized varied widely with some used frequently, and some studies introduced innovative architectures and training methods to optimize performance. A single dataset with 2D slices only was very commonly used.

4.1.1 Automatic Segmentation

Deep Learning Methods

Among the 26 studies using deep learning techniques, 16 employed U-Net-based models. The performance of these models varied, highlighting the importance of dataset quality, preprocessing, and architectural modifications. Modifications such as residual blocks [36], attention mechanisms [32], ensemble learning [28], and optimization techniques [48] helped enhance performance. While PG segmentation remained challenging due to anatomical complexity and small size, models like DeepPGSegNet [31] achieved up to 89%, and PA segmentation with EfficientNet reached 96.41% [45].

Segmentation of Both PA and Residual Healthy PG

Several studies included both PA and residual healthy PG tissue segmentation from the same subjects in their models. These studies are significant because segmenting both structures simultaneously adds complexity due to the differences in size, shape, and tissue contrast between the PA and the normal PG (or residual healthy PG), but is also more clinically significant.

- Wang et al. [26] employed a *Gated-shaped U-Net*, incorporating region-specific gating mechanisms to improve segmentation accuracy, achieving a Dice score of 89.80% for PA segmentation and 60.00% for the PG. The higher performance in PA segmentation was attributed to the PA's larger size and clearer boundaries compared to the smaller and more complex anatomical structure of the residual healthy PG.

- Cerny et al. [29] implemented a fully automated segmentation system using a standard *U-Net* architecture, achieving a high Dice score of 93.4% for PA segmentation and 61.1% for the residual healthy PG. Interestingly, additional pulse sequences did not enhance performance, suggesting that the core architecture was robust enough for PA segmentation without needing extra input modalities.

Advancements and Contributions of Deep Learning Methods

For *PG segmentation*, the consistent challenge across studies has been the small size and indistinct anatomical boundaries of the pituitary gland. Nonetheless, several approaches have yielded promising results. Alzahrani et al. [30] adopted a multi-modal approach, integrating CT and MRI contours into U-Net frameworks, which led to a Dice score of 67%. Mlynarski et al. [25] demonstrated that minor architectural modifications to the conventional U-Net, such as having one segmentation layer per class trained on three planes with majority voting, and allowing for one-voxel mismatch to assess the performance, can improve segmentation performance metrics on small structures, reporting a Dice score of 79%. Building upon architectural enhancements, Gologorsky et al. [28] implemented ensemble learning with a suite of 3D U-Net variants, achieving up to 79% accuracy by leveraging diverse model outputs. Meanwhile, Liu et al. [32] introduced attention mechanisms into their architecture via the Channel Attention Long-Short-Term-Memory (CALN) model, combining Long-Short-Term-Memory (LSTM) and channel attention to enhance fine-grained spatial detail, achieving 84%. The highest performance was observed in the study by Choi et al. [31], whose *DeepPGSegNet* achieved a Dice score of 89% despite being trained on a relatively narrow age cohort, underscoring the potential of deeper, well-optimized U-Net architectures for small structure segmentation.

In contrast, *PA segmentation* presents a broader structural target, especially macroadenomas and giant PAs but still benefits from the adaptability of U-Net-based models. Several studies emphasized architectural optimization to handle variations in adenoma size and morphology. Shu et al. [38] used the dynamic, self-configuring nnU-Net framework to accommodate diverse tumor types, achieving up to 85% Dice, with improved performance on larger lesions. Similarly, Wang et al. [26] employed a gated-shaped U-Net incorporating spatial attention to segment both PA and residual healthy PG tissue, achieving 89% Dice for PA. Jiang et al. [40] addressed feature scaling challenges through a modified U-Net with cross-layer connections, resulting in an 88% Dice score. Cerný et al. [29] demonstrated that even a conventional 3D U-Net, when trained effectively, can achieve excellent performance—reporting a Dice score of

93%, the highest among reviewed studies that did not utilize the Cheng 2015 dataset 2D slices [15].

From a multi-scale learning perspective, *Zhang et al. (2023)* [44] introduced parallel dilated convolutions and attention modules within their Parallel Dilated Convolutional (PDC) U-Net to enhance boundary representation, while *Zhang et al. (2024)* [47] developed Multiscale Residual Network (MSR-Net) with dual decoding paths, attaining Dice scores of 88% and 89%, respectively.

Other studies tackled PA segmentation through model regularization and optimization strategies. Saifullah et al. [48] incorporated Particle Swarm Optimization (PSO) into a CNN-U-Net hybrid to fine-tune hyperparameters such as learning rate and dropout, yielding 92%. *Li et al. (2021)* [36] used a residual U-Net to enhance feature extraction across scales, achieving 80%. Wu et al. [37], in a comparative benchmarking study, observed that U-Net underperformed (7%) relative to deeper architectures such as DeepMedic (29%), illustrating the limitations of basic U-Net models when data is sparse or heterogeneous. The highest Dice score was reported by Rai et al. [45], who designed a dual-headed UNet-EfficientNet model capable of simultaneous classification and segmentation, and further improved performance through post-processing using connected component labeling, reaching 96%.

Other Deep Learning Approaches

Several studies explored deep learning methods beyond the commonly used U-Net architecture, yielding diverse results in PA and PG segmentation. The multiscale feature integration demonstrated by Diaz-Pernas et al. [34] and the progressive refinement strategy of cfVB-Net in *Li et al. (2023)* [42] illustrate how architectural choices can directly address the challenges of segmenting small and variable anatomical structures obtaining Dice scores of 81% and 87% respectively. Gologorsky et al. [28] further highlighted the benefits of ensemble learning, showing how the aggregation of complementary model outputs can yield more robust segmentation outcomes in complex regions like the sellar and para-sellar space achieving a Dice score of 79%.

Comparison with UNet-Based Methods:

Performance Metrics: While U-Net-based architectures delivered strong results—reaching Dice scores as high as 96% in PA segmentation (Rai et al. [45]) and 89% in PG segmentation (Choi et al. [31])—several non-U-Net approaches produced competitive outcomes. For example, the multiscale method by Diaz-Pernas et al. [34] achieved 81%, and the modified QuickNAT model by Maas et al. [35] reached 81%. However, not all alternative architectures matched this performance; Wu et al. [37], working with a limited dataset, reported Dice scores below 40% across several tested models, underscoring the importance of data volume and quality.

Computational Requirements: Architectures such as QuickNAT [58] and the multiscale CNN [34] introduced greater computational demands compared to baseline U-Net models due to their pretraining and structural complexity. While U-Net's design is known for its efficiency and ease of implementation, these advanced methods often rely on more complex layer hierarchies or ensemble strategies. Nevertheless, the added complexity may be warranted in contexts where enhanced sensitivity and specificity are crucial, particularly for variable tumor sizes or boundary detection.

Application Scenarios: A recurring theme among these alternative approaches is their alignment with specialized use cases. *Li et al. (2023)* [42] integrated segmentation with radiomics to predict the Ki67 proliferation index—a clinically relevant biomarker—highlighting the potential of tailored architectures like cfVB-Net in personalized diagnostics. Similarly, *Gologorsky et al. [28]* addressed broader brain region segmentation using diverse volumetric models, reflecting a different operational focus from typical lesion-targeted pipelines.

In summary, while U-Net and its derivatives remain dominant in pituitary segmentation due to their reliability and flexibility, other deep learning strategies offer valuable alternatives in specific scenarios. These models expand the methodological toolkit for handling diverse data characteristics, enhancing performance where traditional architectures may encounter limitations.

Other Automatic Methods

A few studies explored non-deep learning automatic methods. *Isambert et al. [24]* used an atlas-based approach (ABAS), developed from synthetic data [59], for PG segmentation and achieved a low Dice score (30%) due to anatomical variability. In contrast, *Alqhatani et al. [46]* applied Fuzzy C-Means (FCM) clustering with preprocessing enhancements for PA, achieving 95%. These approaches show potential but remain highly dependent on structure type and dataset conditions.

Comparison with Deep Learning Approaches:

The Dice score of 30% reported by *Isambert et al. [24]* using the ABAS atlas-based method highlights the limitations of non-learning approaches in segmenting small structures like the PG, where deep learning models such as U-Net have achieved up to 79% [25] and 89% [31]. While multi-atlas methods may perform comparably to deep learning in other contexts [60], ABAS’s synthetic-anatomy approach performance remains low. *Alqhatani et al. [46]* achieved a high Dice score of 95% for PA segmentation using FCM clustering and enhancement techniques, nearly matching the 96% by *Rai et al. [45]* using a UNet-EfficientNet model. However, both relied on the same dataset [15], potentially inflating performance.

4.1.2 Semi-Automatic Segmentation

Intensity (region-based) segmentation approaches have proven effective in PG and PA delineation, offering an alternative to deep learning when computational resources or annotated datasets are limited. *Zhang et al. [49]* and *Banday & Mir [50]* combined wavelet transforms with mathematical morphology for PA segmentation, achieving Dice scores of 87% and 92%, respectively. For PG, *Zennadi et al. [51]* used SPM12 to create probabilistic atlases from young adult female MRIs, reaching 80% accuracy, though demographic bias was noted [61–63].

Early innovations by *Zukic et al. [52]* and *Egger et al. [53, 54]* applied balloon inflation, Grow-cut, and graph-based methods for PA segmentation, achieving scores between 75% and 81%, respectively. *Sun et al. [55]* combined random walk initialization with active contours to enhance segmentation accuracy (88%). Meanwhile, *Thias et al. [56]* and *Kumar et al. [57]* reported strong results (up to 84%) using active contour and edge-based approaches on the Cheng dataset [15]. These methods demonstrate that

minimal-intervention tools can still yield reliable outcomes, especially for structurally distinct or homogeneous lesions.

4.2 Comparative Analysis

Automatic methods, particularly deep learning-based approaches, generally outperform semi-automatic techniques in segmentation accuracy and multi-region coverage (Figure 5). U-Net variants have achieved high Dice scores (Figure 6). These methods also support simultaneous segmentation of PA and PG, which is clinically useful when analyzing both lesion and healthy tissue.

A key difference lies in user interaction. Automatic models require no input once trained, enabling consistent, rapid inference. Semi-automatic methods like *GrowCut* [53], on the other hand, depend on user input for tasks like boundary marking, which can introduce variability but also enhance precision in challenging cases.

In terms of computational demand, deep learning requires extensive training resources, as highlighted by Wu et al. [37] and Li et al. [42]. Semi-automatic techniques, such as balloon inflation [52] and graph-based active contouring [55], are computationally lighter and suitable for low-resource settings.

Clinically, automated methods suit high-throughput needs, while semi-automatic tools remain relevant where expert guidance is feasible or data are limited. Region-based methods like those by Thias et al. [56] and Kumar et al. [57] still deliver strong performance for focused tasks. Ultimately, data availability remains crucial to deep learning success.

4.3 Challenges and Limitations

Despite promising advances, the studies reviewed exhibit several recurring limitations that impact the interpretability, comparability, and clinical applicability of segmentation models for PG and PA.

One notable challenge is the inconsistent reporting of tumour characteristics—particularly the size of PAs. Many studies, such as Jiang et al. [40] and Gab Allah et al. [39], reported high Dice scores for PA segmentation but did not specify whether the tumors were micro, macro, or giant adenomas. Since larger structures tend to yield higher Dice scores due to clearer anatomical boundaries [60], and lower surface-to-volume-ratios, this lack of stratification limits the ability to fairly assess model performance across different tumor complexities. By contrast, studies such as Shu et al. [38] and *Li et al. (2021)* [36] provided more granular tumor size classifications, offering a more nuanced understanding of model capabilities across lesion types.

Furthermore, the overwhelming reliance on Dice or Jaccard scores—without complementary metrics like Average Symmetric Surface Distance (ASSD)—restricts insight into boundary accuracy, particularly in smaller or irregularly shaped lesions. Although Dice is widely used, the Jaccard index provides a stricter overlap evaluation: $J = \frac{|A \cap B|}{|A \cup B|}$; $D = \frac{2|A \cap B|}{|A| + |B|}$. These metrics are mathematically related as $D = \frac{2J}{1+J}$ and $J = \frac{D}{2-D}$ [64, 65]. Jaccard theoretically controls Dice [66] and offers better numerical discrimination for high overlaps.

Data limitations also remain a common concern. While some studies, such as Cerný et al. [29], leveraged relatively large ($n=521$) internal datasets, most lacked external validation. High-performing models like those in Rai et al. [45] and Alqhatani et al. [46] achieved Dice scores above 95% using the Cheng 2015 dataset, yet their results were not validated on independent clinical data. On the other end of the spectrum, Wu et al. [37] demonstrated how segmentation models trained on relatively small datasets ($n=155$) struggled to perform consistently across architectures, with Dice scores dropping below 40%. These examples underscore the importance of both data diversity and cross-institutional validation when evaluating generalizability.

Another important limitation is the exclusive reliance on MRI as the imaging modality across all studies. While MRI remains the standard for visualizing pituitary structures, none of the reviewed segmentation pipelines incorporated clinical or biochemical data—such as hormonal assays—that are routinely used for adenoma classification and management. Even studies exploring advanced techniques, such as radiomics and predictive modeling in Li et al. (2023) [42], remained constrained to imaging-derived features. The absence of multimodal data integration limits the clinical interpretability and potential diagnostic value of the models.

While semi-automatic methods present an alternative that often requires less data and computational power, they are not without limitations. Algorithms such as Grow-cut [53], random walk-based models [55], and balloon inflation techniques [52] all require varying degrees of user input. Manual initialization introduces inter-operator variability, reducing reproducibility—especially for less experienced users. Additionally, while methods like those proposed by Banday & Mir [50] and Kumar et al. [57] showed high Dice scores, their application remains constrained to relatively homogeneous tumor presentations, with less evidence supporting their effectiveness in complex or ambiguous anatomical cases.

Finally, atlas-based segmentation approaches, while historically useful even in small brain structures such as the piriform cortex [67], also face limitations when applied to PG. Isambert et al. [24] employed a fully automatic pipeline using atlas-based automatic segmentation software (ABAS) - developed from a synthetic MRI [59]. While this approach enabled high anatomical consistency during development, the use of artificially generated data may have introduced domain discrepancies when applied to real clinical images—potentially contributing to the relatively low Dice score of 30% reported for PG segmentation. In contrast, Zennadi et al. [51] (Dice score of 80%) used a maximum probability atlas (MPA) within the SPM environment, requiring multi-step normalization and manual parameter tuning—characteristics that justify its classification under semi-automatic methods.

Collectively, these challenges emphasize the need for larger, diverse, and well-annotated datasets; standardized reporting of tumor features; inclusion of multimodal clinical data; and external validation. As segmentation models advance, these methodological improvements will be critical to ensuring their reliability, generalizability, and eventual clinical adoption.

5 Future Directions

Future work should focus on developing generalizable models for PG and PA segmentation across diverse imaging protocols and populations, supported by large, multi-institutional annotated datasets. Integrating multimodal inputs—such as clinical or endocrine markers—may enhance diagnostic relevance. Semi-automatic tools should minimize operator input via intuitive design. Lastly, standardized benchmarking and external validation are essential for fair comparisons and clinical translation.

6 Conclusion

This review set out to assess the accuracy of automated segmentation algorithms for pituitary adenomas (PA) and the pituitary gland (PG). Deep learning models—particularly U-Net variants—have shown strong performance, with reported Dice scores reaching 96% for PA and 89% for PG, indicating high accuracy and clinical promise.

Many studies lacked tumor size stratification or external validation, limiting the generalizability of results. Semi-automatic methods remain relevant where data or computational resources are limited, achieving Dice scores above 80% in focused applications.

Overall, automated segmentation tools are increasingly accurate and scalable, but their clinical adoption will depend on improvements in dataset diversity, external validation, and integration with clinical workflows. Answering these challenges is essential for reliable, real-world use in diagnosis, treatment planning, and monitoring of pituitary disorders.

Acknowledgements. We would like to thank Dr. Ayisha Al-Busaidi, Consultant Neuroradiologist at King’s College Hospital London, for her valuable clinical guidance and expertise throughout this review.

6.1 Registration and Protocol

This study is registered with PROSPERO under registration ID CRD42023407127. We adhered as closely as possible to the PRISMA guidelines. We utilized its framework to ensure rigor and transparency in our systematic review process. This included comprehensive search strategies, clearly defined inclusion and exclusion criteria, and a structured approach to data extraction and synthesis.

6.2 Support

The primary author is a PhD student funded by the Africa International Postgraduate Research (PGR) Scholarship, provided by the Centre for Doctoral Studies at King’s College London.

The School of Biomedical Engineering and Imaging Sciences is supported by the Wellcome EPSRC Centre for Medical Engineering at King’s College London (WT 203148/Z/16/Z) and the Department of Health via the National Institute for Health

Research (NIHR) comprehensive Biomedical Research Centre award to Guy's & St Thomas' NHS Foundation Trust in partnership with King's College London and King's College Hospital NHS Foundation Trust. For the purposes of open access, the authors have applied a Creative Commons Attribution (CC BY) licence to any Accepted Author Manuscript version arising, in accordance with King's College London's Rights Retention policy.

6.3 Competing Interest

The authors have no competing interests to declare.

Declarations

The authors have no conflicts of interest to disclose.

Appendix A Studies Included by Inclusion Criteria but Excluded Later

Table A1 provides a summary of the studies that were initially included based on the inclusion criteria but were subsequently excluded after a full-text review. The reasons for exclusion are highlighted in the Table.

Table A1: Summary of Studies Excluded After Full-Text Review

Reason for Exclusion	Study
No segmentation results for PG or PA provided	[68], [69], [70], [71], [72], [73], [74], [75], [76], [77], [78], [79], [80], [81], [82], [83], [84], [85], [86], [87], [88], [89], [90], [91], [92], [93], [94], [95], [96], [97], [98], [99], [100], [101], [102], [103], [104], [105], [106], [107], [108], [109], [110], [111], [112], [113], [110]
No overlap metrics provided	[114], [115], [116]
Similar approach with a more detailed study already included	[117], [118], [119]
Book chapter	[120], [121]
Segmentation results derived from non-standard Dice and Jaccard formulas	[122]
Retracted Study	[123]

References

- [1] Tsukamoto, T., Miki, Y.: Imaging of pituitary tumors: an update with the 5th WHO classifications—part 1. pituitary neuroendocrine tumor (pitNET)/pituitary adenoma. *Japanese Journal of Radiology* **41**(8), 789–806 (2023)
- [2] Ezzat, S., Asa, S.L., Couldwell, W.T., Barr, C.E., Dodge, W.E., Vance, M.L., McCutcheon, I.E.: The prevalence of pituitary adenomas: a systematic review. *Cancer: Interdisciplinary International Journal of the American Cancer Society* **101**(3), 613–619 (2004)
- [3] Molitch, M.E.: Diagnosis and treatment of pituitary adenomas: a review. *Jama* **317**(5), 516–524 (2017)
- [4] Castle-Kirschbaum, M., Amukotuwa, S., Fuller, P., Goldschlager, T., Gonzalvo, A., Kam, J., Kow, C., Shi, M., Stuckey, S.: MRI for Cushing disease: A systematic review. *American Journal of Neuroradiology* **44**(3), 311–316 (2023)
- [5] Chaichana, K.L., Hwang, B.Y.-J., Raza, S.M., Quiñones-Hinojosa, A.: The role of surgery in nonfunctioning pituitary macroadenomas. *Controversies in Neuro-Oncology*, 337 (2013)
- [6] Yildiz, F., Zorlu, F., Erbaş, T., Atahan, L.: Radiotherapy in the management of giant pituitary adenomas. *Radiotherapy and Oncology* **52**(3), 233–237 (1999)
- [7] Molitch, M.E.: Pituitary incidentalomas. *Best Practice & Research Clinical Endocrinology & Metabolism* **23**(5), 667–675 (2009)
- [8] Davies, B.M., Carr, E., Soh, C., Gnanalingham, K.K.: Assessing size of pituitary adenomas: a comparison of qualitative and quantitative methods on MR. *Acta Neurochirurgica* **158**, 677–683 (2016)
- [9] Yao, A., Balchandani, P., Shrivastava, R.K.: Metabolic in vivo visualization of pituitary adenomas: a systematic review of imaging modalities. *World Neurosurgery* **104**, 489–498 (2017)
- [10] Chatain, G.P., Patronas, N., Smirniotopoulos, J.G., Piazza, M., Benzo, S., Ray-Chaudhury, A., Sharma, S., Lodish, M., Nieman, L., Stratakis, C.A., et al.: Potential utility of FLAIR in MRI-negative Cushing's disease. *Journal of Neurosurgery* **129**(3), 620–628 (2017)
- [11] Buchfelder, M., Schlaffer, S.-M.: Modern imaging of pituitary adenomas. *Pituitary Today II* **38**, 109–120 (2010)
- [12] Niendorf, H., Laniado, M., Semmler, W., Schörner, W., Felix, R.: Dose administration of gadolinium-DTPA in MR imaging of intracranial tumors. *American Journal of Neuroradiology* **8**(5), 803–815 (1987)

- [13] Bashari, W.A., Senanayake, R., Fernández-Pombo, A., Gillett, D., Koulouri, O., Powlson, A.S., Matys, T., Scoffings, D., Cheow, H., Mendichovszky, I., *et al.*: Modern imaging of pituitary adenomas. *Best practice & research Clinical endocrinology & metabolism* **33**(2), 101278 (2019)
- [14] Ntali, G., Wass, J.A.: Epidemiology, clinical presentation and diagnosis of non-functioning pituitary adenomas. *Pituitary* **21**, 111–118 (2018)
- [15] Cheng, J.: Brain tumor dataset. figshare. Dataset **1512427**(5) (2017)
- [16] Cheng, J., Huang, W., Cao, S., Yang, R., Yang, W., Yun, Z., Wang, Z., Feng, Q.: Enhanced performance of brain tumor classification via tumor region augmentation and partition. *PloS one* **10**(10), 0140381 (2015)
- [17] Pham, D.L., Xu, C., Prince, J.L.: Current methods in medical image segmentation. *Annual review of biomedical engineering* **2**(1), 315–337 (2000)
- [18] Ramesh, K., Kumar, G.K., Swapna, K., Datta, D., Rajest, S.S.: A review of medical image segmentation algorithms. *EAI Endorsed Transactions on Pervasive Health and Technology* **7**(27), 6–6 (2021)
- [19] Ronneberger, O., Fischer, P., Brox, T.: U-net: Convolutional networks for biomedical image segmentation. In: *Medical Image Computing and Computer-assisted intervention–MICCAI 2015: 18th International Conference, Munich, Germany, October 5–9, 2015, Proceedings, Part III* 18, pp. 234–241 (2015). Springer
- [20] Wang, T.-W., Hsu, M.-S., Lee, W.-K., Pan, H.-C., Yang, H.-C., Lee, C.-C., Wu, Y.-T.: Brain metastasis tumor segmentation and detection using deep learning algorithms: a systematic review and meta-analysis. *Radiotherapy and Oncology*, 110007 (2023)
- [21] Havaei, M., Davy, A., Warde-Farley, D., Biard, A., Courville, A., Bengio, Y., Pal, C., Jodoin, P.-M., Larochelle, H.: Brain tumor segmentation with deep neural networks. *Medical image analysis* **35**, 18–31 (2017)
- [22] Page, M.J., McKenzie, J.E., Bossuyt, P.M., Boutron, I., Hoffmann, T.C., Mulrow, C.D., Shamseer, L., Tetzlaff, J.M., Akl, E.A., Brennan, S.E., *et al.*: The prisma 2020 statement: an updated guideline for reporting systematic reviews-declaracion prisma 2020: una guia actualizada para la publicacion de revisiones sistematicas. *Revista Panamericana de Salud Publica= Pan American Journal of Public Health* **46**, 112–112 (2022)
- [23] Ouzzani, M., Hammady, H., Fedorowicz, Z., Elmagarmid, A.: Rayyan—a web and mobile app for systematic reviews. *Systematic reviews* **5**, 1–10 (2016)
- [24] Isambert, A., Dhermain, F., Bidault, F., Commowick, O., Bondiau, P.-Y.,

Malandain, G., Lefkopoulos, D.: Evaluation of an atlas-based automatic segmentation software for the delineation of brain organs at risk in a radiation therapy clinical context. *Radiotherapy and Oncology* **87**(1), 93–99 (2008)

[25] Mlynarski, P., Delingette, H., Alghamdi, H., Bondiau, P.-Y., Ayache, N.: Anatomically consistent cnn-based segmentation of organs-at-risk in cranial radiotherapy. *Journal of Medical Imaging* **7**(1), 014502–014502 (2020)

[26] Wang, H., Zhang, W., Li, S., Fan, Y., Feng, M., Wang, R.: Development and evaluation of deep learning-based automated segmentation of pituitary adenoma in clinical task. *The Journal of Clinical Endocrinology & Metabolism* **106**(9), 2535–2546 (2021)

[27] Maruyama, T., Hayashi, N., Sato, Y., Ogura, T., Uehara, M., Ogura, A., Watanabe, H., Kitoh, Y., Initiative, A.D.N.: Simultaneous brain structure segmentation in magnetic resonance images using deep convolutional neural networks. *Radiological Physics and Technology* **14**, 358–365 (2021)

[28] Gologorsky, R., Harake, E., Oiste, G., Nasir-Moin, M., Couldwell, W., Oermann, E., Hollon, T.: Generating novel pituitary datasets from open-source imaging data and deep volumetric segmentation. *Pituitary* **25**(6), 842–853 (2022)

[29] Černý, M., Kybic, J., Májovský, M., Sedlák, V., Pirgl, K., Misiorzová, E., Lipina, R., Netuka, D.: Fully automated imaging protocol independent system for pituitary adenoma segmentation: a convolutional neural network—based model on sparsely annotated mri. *Neurosurgical Review* **46**(1), 116 (2023)

[30] Alzahrani, N., Henry, A., Clark, A., Murray, L., Nix, M., Al-Qaisieh, B.: Geometric evaluations of ct and mri based deep learning segmentation for brain oars in radiotherapy. *Physics in Medicine & Biology* **68**(17), 175035 (2023)

[31] Choi, U.-S., Sung, Y.-W., Ogawa, S.: deeppgsegnet: Mri-based pituitary gland segmentation using deep learning. *Frontiers in Endocrinology* **15**, 1338743 (2024)

[32] Liu, J., Sun, Z., Guo, Q., Liu, B., Fu, T., Ma, G., Song, H., Yang, J.: Caln: Channel attention lstm network for pituitary segmentation in dynamic contrast-enhanced mri. In: 2024 IEEE International Symposium on Biomedical Imaging (ISBI), pp. 1–5 (2024). IEEE

[33] Guo, T., Luan, J., Gao, J., Liu, B., Shen, T., Yu, H., Ma, G., Wang, K.: Computer-aided diagnosis of pituitary microadenoma on dynamic contrast-enhanced mri based on spatio-temporal features. *Expert Systems with Applications* **260**, 125414 (2025)

[34] Díaz-Pernas, F.J., Martínez-Zarzuela, M., Antón-Rodríguez, M., González-Ortega, D.: A deep learning approach for brain tumor classification and

segmentation using a multiscale convolutional neural network. *Healthcare* **9**(2), 153 (2021)

- [35] Maas, B., Zabeh, E., Arabshahi, S.: Quicktumornet: fast automatic multi-class segmentation of brain tumors. In: 2021 10th International IEEE/EMBS Conference on Neural Engineering (NER), pp. 81–85 (2021). IEEE
- [36] Li, H., Zhao, Q., Zhang, Y., Sai, K., Xu, L., Mou, Y., Xie, Y., Ren, J., Jiang, X.: Image-driven classification of functioning and nonfunctioning pituitary adenoma by deep convolutional neural networks. *Computational and Structural Biotechnology Journal* **19**, 3077–3086 (2021)
- [37] Wu, S., Wu, Y., Chang, H., Su, F.T., Liao, H., Tseng, W., Liao, C., Lai, F., Hsu, F., Xiao, F.: Deep learning-based segmentation of various brain lesions for radiosurgery. *Applied Sciences* **11**(19), 9180 (2021)
- [38] Shu, X., Zhou, Y., Li, F., Zhou, T., Meng, X., Wang, F., Zhang, Z., Pu, J., Xu, B.: Three-dimensional semantic segmentation of pituitary adenomas based on the deep learning framework-nnu-net: A clinical perspective. *Micromachines* **12**(12), 1473 (2021)
- [39] Allah, A.M.G., Sarhan, A.M., Elshennawy, N.M.: Edge u-net: Brain tumor segmentation using mri based on deep u-net model with boundary information. *Expert Systems with Applications* **213**, 118833 (2023)
- [40] Jiang, X., Xiao, J., Zhang, Q., Wang, L., Jiang, J., Lan, K.: Improved u-net based on cross-layer connection for pituitary adenoma mri image segmentation. *Mathematical biosciences and engineering: MBE* **20**(1), 34–51 (2022)
- [41] Razzaghi, P., Abbasi, K., Shirazi, M., Rashidi, S.: Multimodal brain tumor detection using multimodal deep transfer learning. *Applied Soft Computing* **129**, 109631 (2022)
- [42] Li, H., Liu, Z., Li, F., Shi, F., Xia, Y., Zhou, Q., Zeng, Q.: Preoperatively predicting ki67 expression in pituitary adenomas using deep segmentation network and radiomics analysis based on multiparameter mri. *Academic Radiology* **31**(2), 617–627 (2023)
- [43] Da Mutten, R., Zanier, O., Ciobanu-Caraus, O., Voglis, S., Hugelshofer, M., Pangalau, A., Regli, L., Serra, C., Staartjes, V.E.: Automated volumetric assessment of pituitary adenoma. *Endocrine* **83**(1), 171–177 (2024)
- [44] Zhang, Q., Cheng, J., Zhou, C., Jiang, X., Zhang, Y., Zeng, J., Liu, L.: Pdcnet: parallel dilated convolutional network with channel attention mechanism for pituitary adenoma segmentation. *Frontiers in Physiology* **14**, 1259877 (2023)
- [45] Rai, H.M., Yoo, J., Dashkevych, S.: Two-headed unetefficientnets for parallel

execution of segmentation and classification of brain tumors: Incorporating post-processing techniques with connected component labelling. *Journal of Cancer Research and Clinical Oncology* **150**(4), 220 (2024)

- [46] Alqhtani, S.M., Soomro, T.A., Ali, A., Aziz, A., Irfan, M., Rahman, S., Jalalah, M., Almawgani, A.H., Eljak, L.A.B.: Improved brain tumor segmentation and classification in brain mri with fcm-svm: a diagnostic approach. *IEEE Access* (2024)
- [47] Zhang, Q., Jiang, X., Huang, X., Zhou, C.: Msr-net: Multi-scale residual network based on attention mechanism for pituitary adenoma mri image segmentation. *IEEE Access* (2024)
- [48] Saifullah, S., Dreżewski, R.: Automatic brain tumor segmentation using convolutional neural networks: U-net framework with pso-tuned hyperparameters. In: *International Conference on Parallel Problem Solving from Nature*, pp. 333–351 (2024). Springer
- [49] Zhang, X., Liu, X., Lin, W.: Computing optimization technique in enhancing magnetic resonance imaging and brain segmentation of hypophysis cerebri based on morphological based image processing. *Journal of Medical Imaging and Health Informatics* **6**(4), 1063–1070 (2016)
- [50] Banday, S.A., Mir, A.H.: Enhancement and segmentation of pituitary gland from mr brain images. *International Journal of Medical Engineering and Informatics* **9**(3), 201–219 (2017)
- [51] Zennadi, M.M., Ptito, M., Redouté, J., Costes, N., Boutet, C., Germain, N., Galusca, B., Schneider, F.C.: Mri atlas of the pituitary gland in young female adults. *Brain Structure and Function* **229**(4), 1001–1010 (2024)
- [52] Zukic, D., Egger, J., Bauer, M.H., Kuhnt, D., Carl, B., Freisleben, B., Kolb, A., Nimsky, C.: Preoperative volume determination for pituitary adenoma. In: *Medical Imaging 2011: Computer-Aided Diagnosis*, vol. 7963, pp. 817–823. SPIE, ??? (2011)
- [53] Egger, J., Kapur, T., Nimsky, C., Kikinis, R.: Pituitary adenoma volumetry with 3d slicer. *PLOS ONE* **7**(12), 51788 (2012)
- [54] Egger, J., Zukić, D., Freisleben, B., Kolb, A., Nimsky, C.: Segmentation of pituitary adenoma: A graph-based method vs. a balloon inflation method. *Computer Methods and Programs in Biomedicine* **110**(3), 268–278 (2013)
- [55] Sun, M., Chen, X., Zhang, Z., Ma, C.: Random walk and graph cut based active contour model for three-dimension interactive pituitary adenoma segmentation from mr images. In: *Medical Imaging 2017: Image Processing*, vol. 10133, pp. 548–555. SPIE, ??? (2017)

[56] Thias, A.H., Al Mubarok, A.F., Handayani, A., Danudirdjo, D., Rajab, T.E.: Brain tumor semi-automatic segmentation on mri t1-weighted images using active contour models. In: 2019 International Conference on Mechatronics, Robotics and Systems Engineering (MoRSE), pp. 217–221. IEEE, ??? (2019)

[57] Kumar, S.B., Panda, R., Agrawal, S.: Brain magnetic resonance image tumor detection and segmentation using edgeless active contour. In: 2020 11th International Conference on Computing, Communication and Networking Technologies (ICCCNT), pp. 1–7 (2020). IEEE

[58] Roy, A.G., Conjeti, S., Navab, N., Wachinger, C., Initiative, A.D.N., *et al.*: Quicknat: A fully convolutional network for quick and accurate segmentation of neuroanatomy. *NeuroImage* **186**, 713–727 (2019)

[59] Bondiau, P.-Y., Malandain, G., Chanalet, S., Marcy, P.-Y., Habrand, J.-L., Fau-chon, F., Paquis, P., Courdi, A., Commowick, O., Rutten, I., *et al.*: Atlas-based automatic segmentation of mr images: validation study on the brainstem in radiotherapy context. *International Journal of Radiation Oncology* Biology* Physics* **61**(1), 289–298 (2005)

[60] Yaakub, S.N., Heckemann, R.A., Keller, S.S., McGinnity, C.J., Weber, B., Hammers, A.: On brain atlas choice and automatic segmentation methods: a comparison of maper & freesurfer using three atlas databases. *Scientific Reports* **10**(1), 2837 (2020)

[61] Doraiswamy, P.M., Potts, J.M., Axelson, D.A., Husain, M.M., Lurie, S.N., Na, C., Escalona, P.R., McDonald, W.M., Fiegel, G.S., Ellinwood, E.: Mr assessment of pituitary gland morphology in healthy volunteers: age-and gender-related differences. *American Journal of Neuroradiology* **13**(5), 1295–1299 (1992)

[62] Ikram, M.F., Sajjad, Z., Shokh, I., Omair, A.: Pituitary height on magnetic resonance imaging observation of age and sex related changes. *JPMA. The Journal of the Pakistan Medical Association* **58**(5), 261 (2008)

[63] Lamichhane, T.R., Pangeni, S., Paudel, S., Lamichhane, H.P.: Age and gender related variations of pituitary gland size of healthy nepalese people using magnetic resonance imaging. *Am J Biomed Eng* **5**(4), 130–135 (2015)

[64] Jaccard, P.: La distribution de la flore dans la zone alpine. *Revue Générale des Sciences Pures et Appliquées* **18**(23), 961–967 (1907)

[65] Dice, L.R.: Measures of the amount of ecologic association between species. *Ecology* **26**(3), 297–302 (1945)

[66] Bertels, J., Eelbode, T., Berman, M., Vandermeulen, D., Maes, F., Bisschops, R., Blaschko, M.B.: Optimizing the dice score and jaccard index for medical image segmentation: Theory and practice. In: *Medical Image Computing and*

Computer Assisted Intervention–MICCAI 2019: 22nd International Conference, Shenzhen, China, October 13–17, 2019, Proceedings, Part II 22, pp. 92–100 (2019). Springer

- [67] Steinbart, D., Yaakub, S.N., Steinbrenner, M., Guldin, L.S., Holtkamp, M., Keller, S.S., Weber, B., Rüber, T., Heckemann, R.A., Ilyas-Feldmann, M., *et al.*: Automatic and manual segmentation of the piriform cortex: Method development and validation in patients with temporal lobe epilepsy and alzheimer’s disease. *Human Brain Mapping* **44**(8), 3196–3209 (2023)
- [68] Kumar, S., Kumar, D.: Human brain tumor classification and segmentation using cnn. *Multimedia Tools and Applications* **82**(5), 7599–7620 (2023)
- [69] Hashmi, A., Osman, A.H.: Brain tumor classification using conditional segmentation with residual network and attention approach by extreme gradient boost. *Applied Sciences* **12**(21), 10791 (2022)
- [70] Divya, S., Padma Suresh, L., John, A.: Enhanced deep-joint segmentation with deep learning networks of glioma tumor for multi-grade classification using mr images. *Pattern Analysis and Applications* **25**(4), 891–911 (2022)
- [71] Alnaggar, O., Jagadale, B.N., Narayan, S.H.: Mri brain tumor detection using boosted crossbred random forests and chimp optimization algorithm based convolutional neural networks. *Int J Intell Eng Syst* **15**(2), 36–46 (2022)
- [72] Balamurugan, T., Gnanamanoharan, E.: Genetic algorithm and deep learning feature based tumor detection. *Indian Journal of Computer Science and Engineering* **12**(6), 1837–1846 (2021)
- [73] Kalam, R., Thomas, C., Rahiman, M.A.: Detection of brain tumor in mri images using optimized anfis classifier. *International Journal of Uncertainty, Fuzziness and Knowledge-Based Systems* **29**(Supp01), 1–29 (2021)
- [74] Pranav, P., Samhita, P.: Automated computer-aided diagnosis for brain tumor detection. In: 2021 13th Biomedical Engineering International Conference (BMEiCON), pp. 1–5 (2021). IEEE
- [75] Gupta, S., Punn, N.S., Sonbhadra, S.K., Agarwal, S.: Mag-net: Multi-task attention guided network for brain tumor segmentation and classification. In: Big Data Analytics: 9th International Conference, BDA 2021, Virtual Event, December 15–18, 2021, Proceedings 9, pp. 3–15 (2021). Springer
- [76] Isunuri, B.V., Kakarla, J.: Brain tumor extraction using adaptive threshold selection network. In: 2019 IEEE 1st International Conference on Energy, Systems and Information Processing (ICESIP), pp. 1–6 (2019). IEEE
- [77] Egger, J., Kappus, C., Freisleben, B., Nimsky, C.: A medical software system for

volumetric analysis of cerebral pathologies in magnetic resonance imaging (mri) data. *Journal of medical systems* **36**, 2097–2109 (2012)

[78] Wisaeng, K., Sa-Ngiamvibool, W.: Brain tumor segmentation using fuzzy otsu threshold morphological algorithm. *IAENG International Journal of Applied Mathematics* **53**(2), 1–12 (2023)

[79] Jeribi, F., Perumal, U.: Lesion detection based bt type classification model using svt-kld-fcm and vcr-50. In: *International Conference on Computing and Information Technology*, pp. 11–25 (2023). Springer

[80] Abd Al Hussen, S.A., Alsaadi, E.M.T.A.: Automated identification and classification of brain tumors using hybrid machine learning models and mri imaging. *Ingenierie des Systemes d'Information* **28**(5), 1299 (2023)

[81] Sahoo, A.K., Parida, P., Muralibabu, K., Dash, S.: Efficient simultaneous segmentation and classification of brain tumors from mri scans using deep learning. *Biocybernetics and Biomedical Engineering* **43**(3), 616–633 (2023)

[82] Singh, N.T., Kaur, P., Chaudhary, A., Singla, S.: Detection of brain tumors through the application of deep learning and machine learning models. In: *2023 IEEE 8th International Conference for Convergence in Technology (I2CT)*, pp. 1–6 (2023). IEEE

[83] Singh, Y.P., Lobiyal, D.: A comparative analysis and classification of cancerous brain tumors detection based on classical machine learning and deep transfer learning models. *Multimedia Tools and Applications* **83**(13), 39537–39562 (2024)

[84] Krishnasamy, N., Ponnusamy, T.: Deep learning-based robust hybrid approaches for brain tumor classification in magnetic resonance images. *International Journal of Imaging Systems and Technology* **33**(6), 2157–2177 (2023)

[85] Vizza, P., Cannistrà, M., Giancotti, R., Veltri, P.: Image processing segmentation algorithms evaluation through implementation choices. In: *Proceedings of the 13th ACM International Conference on Bioinformatics, Computational Biology and Health Informatics*, pp. 1–7 (2022)

[86] Chaki, J., Woźniak, M.: A deep learning based four-fold approach to classify brain mri: Btsenet. *Biomedical Signal Processing and Control* **85**, 104902 (2023)

[87] Muis, A., Sunardi, S., Yudhana, A.: Comparison analysis of brain image classification based on thresholding segmentation with convolutional neural network. *Journal of Applied Engineering and Technological Science (JAETS)* **4**(2), 664–673 (2023)

[88] Singh, G., Gautam, V.: Pituitary gland size estimation and lesion detection

using segmentation-based color thresholding technique. In: 2023 International Conference on Sustainable Computing and Smart Systems (ICSCSS), pp. 700–704 (2023). IEEE

[89] Gupta, A., Dixit, M., Mishra, V.K., Singh, A., Dayal, A.: Brain tumor segmentation from mri images using deep learning techniques. In: International Advanced Computing Conference, pp. 434–448 (2023). Springer

[90] Abd Al Hussen, S.A., Alsaadi, E.M.T.A.: Automated identification and classification of brain tumors using hybrid machine learning models and mri imaging. *Ingenierie des Systemes d'Information* **28**(5), 1299 (2023)

[91] Kordnoori, S., Sabeti, M., Shakoor, M.H., Moradi, E.: Deep multi-task learning structure for segmentation and classification of supratentorial brain tumors in mr images. *Interdisciplinary Neurosurgery* **36**, 101931 (2024)

[92] Muhammad, S.D., Kobti, Z.: An ensemble deep learning approach for enhanced classification of pituitary tumors. In: 2023 IEEE Symposium Series on Computational Intelligence (SSCI), pp. 427–432 (2023). IEEE

[93] Kotti, J., Moovendran, M., Kandasamy, M.: Multi-level brain tumor classification using hybrid coot flamingo search optimization algorithm enabled deep learning with mri images. *Network: Computation in Neural Systems*, 1–32 (2024)

[94] Shanthala, K., Chandrakala, B., Shobha, N., *et al.*: Automated diagnosis of brain tumor classification and segmentation of mri images. In: 2023 International Conference on the Confluence of Advancements in Robotics, Vision and Interdisciplinary Technology Management (IC-RVITM), pp. 1–7 (2023). IEEE

[95] Krishnan, P.L.B.M., Sampath, V.: A multiscale morphological segmentation and classification of brain tumor using supervised learning algorithm. In: AIP Conference Proceedings, vol. 2966 (2024). AIP Publishing

[96] Mehta, B., Sharma, R., Kumar, S., Chauhan, S.S., Bhatnagar, V.: Computer vision tools for tumor segmentation. In: High Energy Physics Symposium, pp. 550–554 (2022). Springer

[97] Dénes-Fazekas, L., Kovács, L., Eigner, G., Szilágyi, L.: Brain tumor segmentation from multi-spectral mri records using a u-net cascade architecture. In: 2023 IEEE International Conference on Systems, Man, and Cybernetics (SMC), pp. 3003–3008 (2023). IEEE

[98] Belaid, O.N., Loudini, M., Nakib, A.: Brain tumor classification using densenet and u-net convolutional neural networks. In: 2024 8th International Conference on Image and Signal Processing and Their Applications (ISPA), pp. 1–6 (2024). IEEE

[99] Roy, S., Mandal, B.K., Khamaru, K., Bhattacharya, A.: Prediction and classification of brain tumor using modified transfer learning. In: 2024 11th International Conference on Computing for Sustainable Global Development (INDIACoM), pp. 850–854 (2024). IEEE

[100] Kumar, Y., Badiger, V.S., Shyam, G.K., *et al.*: Brain tumour segmentation and classification using the convolutional neural network (u-net model). In: 2023 International Conference on Advanced Computing & Communication Technologies (ICACCTech), pp. 258–265 (2023). IEEE

[101] Rosa, S., Vasconcelos, V., Caridade, P.J.: Evaluating the impact of filtering techniques on deep learning-based brain tumour segmentation. *Computers* **13**(9), 237 (2024)

[102] Kumar, P.R., Bonthu, K., Meghana, B., Vani, K.S., Chakrabarti, P.: Multi-class brain tumor classification and segmentation using hybrid deep learning network model. *Scalable Computing: Practice and Experience* **24**(1), 69–80 (2023)

[103] Geetha, M., Srinadh, V., Janet, J., Sumathi, S.: Hybrid archimedes sine cosine optimization enabled deep learning for multilevel brain tumor classification using mri images. *Biomedical Signal Processing and Control* **87**, 105419 (2024)

[104] Waghene, S.S., Shinde, J.P.: A robust classification of brain tumor disease in mri using twin-attention based dense convolutional auto-encoder. *Biomedical Signal Processing and Control* **92**, 106088 (2024)

[105] Li, G., Hui, X., Li, W., Luo, Y.: Multitask learning with multiscale residual attention for brain tumor segmentation and classification. *Machine Intelligence Research* **20**(6), 897–908 (2023)

[106] Alshomrani, F.: A unified pipeline for simultaneous brain tumor classification and segmentation using fine-tuned cnn and residual unet architecture. *Life* **14**(9), 1143 (2024)

[107] Andleeb, I., Hussain, B.Z., Ansari, S., Ansari, M.S., Kanwal, N., Aslam, A.: Deep learning based lightweight model for brain tumor classification and segmentation. In: UK Workshop on Computational Intelligence, pp. 491–503 (2023). Springer

[108] Jader, R.F., Kareem, S.W., Awla, H.Q.: Ensemble deep learning technique for detecting mri brain tumor. *Applied Computational Intelligence and Soft Computing* **2024**(1), 6615468 (2024)

[109] Shirwaikar, R.D., Ramesh, K., Faisal, A.M., Jeshwanth, M., Raghav, A.: 3d segmentation of brain tumour. *International Journal of Engineering Systems Modelling and Simulation* **15**(2), 76–83 (2024)

- [110] Sindhu, S., Vijayalakshmi, N.: The elevation of efficacy identifying pituitary tissue abnormalities within brain images by employing memory contrast learning techniques. *Journal of applied mathematics & informatics* **42**(4), 931–943 (2024)
- [111] Yan, X., Lin, B., Fu, J., Li, S., Wang, H., Fan, W., Fan, Y., Feng, M., Wang, R., Fan, J., *et al.*: Deep-learning-based automatic segmentation and classification for craniopharyngiomas. *Frontiers in Oncology* **13**, 1048841 (2023)
- [112] Gargya, S., Jain, S.: Cad system design for pituitary tumor classification based on transfer learning technique. *Current Medical Imaging* **20**(1), 15734056246146 (2024)
- [113] Almufareh, M.F., Imran, M., Khan, A., Humayun, M., Asim, M.: Automated brain tumor segmentation and classification in mri using yolo-based deep learning. *IEEE Access* **12**, 16189–16207 (2024)
- [114] Renz, D.M., Hahn, H.K., Schmidt, P., Rexilius, J., Lentschig, M., Pfeil, A., Sauner, D., Fitzek, C., Mentzel, H.-J., Kaiser, W.A., *et al.*: Accuracy and reproducibility of a novel semi-automatic segmentation technique for mr volumetry of the pituitary gland. *Neuroradiology* **53**, 233–244 (2011)
- [115] Wong, A.P.-Y., Pipitone, J., Park, M.T.M., Dickie, E.W., Leonard, G., Perron, M., Pike, B.G., Richer, L., Veillette, S., Chakravarty, M.M., *et al.*: Estimating volumes of the pituitary gland from t1-weighted magnetic-resonance images: effects of age, puberty, testosterone, and estradiol. *Neuroimage* **94**, 216–221 (2014)
- [116] Al Hinai, Q., Mok, K., Zeitouni, A., Gagnon, B., Ajlan, A.R., Rivera, J., Tewfik, M., Sirhan, D.: Comparison between manual and semiautomated volumetric measurements of pituitary adenomas. *Skull Base* **21**(06), 365–372 (2011)
- [117] Alqhtani, S.M., Soomro, T.A., Ali, A., Irfan, M., Asiri, A.A., *et al.*: Contrast normalization strategies in brain tumor imaging: From preprocessing to classification. *CMES Computer Modeling in Engineering and Sciences* **140**(2) (2024)
- [118] Asiri, A.A., Soomro, T.A., Shah, A.A., Pogrebna, G., Irfan, M., Alqahtani, S.: Optimized brain tumor detection: a dual-module approach for mri image enhancement and tumor classification. *IEEE Access* **12**, 42868–42887 (2024)
- [119] Li, H., Liu, Z., Li, F., Xia, Y., Zhang, T., Shi, F., Zeng, Q.: Identification of prolactinoma in pituitary neuroendocrine tumors using radiomics analysis based on multiparameter mri. *Journal of Imaging Informatics in Medicine*, 1–9 (2024)
- [120] Abinash, V., Meghanth, S., Rakesh, P., Sajidha, S., Nisha, V., Muralidhar, A.: An efficient transfer learning-based cnn multi-label classification and resunet based segmentation of brain tumor in mri. In: *Recurrent Neural Networks*, pp.

247–262. CRC Press, Boca Raton, FL (2022)

- [121] Rajagopal, R., Jose, S.E.: An efficient framework for locating stroke in brain mri images using radon transform and convolutional neural networks. In: Next Generation of Internet of Things: Proceedings of ICNGIoT 2021, pp. 385–395 (2021). Springer
- [122] Sunsuhi, G., Jose, S.A.: An adaptive eroded deep convolutional neural network for brain image segmentation and classification using inception resnetv2. *Biomedical Signal Processing and Control* **78**, 103863 (2022)
- [123] Haq, E.U., Jianjun, H., Huarong, X., Li, K., Weng, L.: [retracted] a hybrid approach based on deep cnn and machine learning classifiers for the tumor segmentation and classification in brain mri. *Computational and Mathematical Methods in Medicine* **2022**(1), 6446680 (2022)